DOI: 10.61782/fa.2025.0831

FORUM ACUSTICUM EURONOISE 2025

STREAMING OVER MICRO-PERFORATED WALLS SUBMITTED TO ACOUSTIC PLANE WAVE

Daniel Mazzoni[1*] **Muriel Amielh**[1] **Loane Genevay**[1]
Teresa Bravo[2] **Cédric Maury**[3]
[1] Aix Marseille Univ, CNRS, Centrale Méditerranée, IRPHE UMR 7342, 13384, Marseille, France
[2] ITEFI, Consejo Superior de Investigaciones Cientificas, Madrid, 28006, Spain
[3] Aix Marseille Univ, CNRS, Centrale Méditerranée, LMA UMR 7031, 13013, Marseille, France

ABSTRACT

Micro-perforated panels (MPPs), lightweight structures, are investigated as alternatives to huge or active devices, to attenuate noise induced by external flow into the passenger compartment of automobile or aircraft cabins. Optimal sound absorption performance is achieved by appropriate selection of MPP geometry. The viscous losses through the apertures dissipate the acoustic energy around the Helmholtz resonance and provide high absorption efficiency over a wide bandwidth. Acoustically induced vorticity, due to streaming at the hole inlet/outlet, could also contribute. The experiment quantifies the flow induced by acoustic pressure fluctuations (”streaming”) in the vicinity of the perforations of an MPP placed on a cavity arranged on the wall of a closed tube. Three diameters of perforations ($1mm$, $0.6mm$ and $0.3mm$) are tested. The flow induced by an acoustic plane wave parallel to the surface of the MPP is characterized by TR-PIV (”Time Resolved Particle Image Velocimetry”), a laser optical diagnostics, synchronized with acoustic measurements by microphone. The dynamics of the jets emitted at the holes according to their relative position to the wavelength associated with different identified eigenmodes of the closed tube is highlighted. The objective is to estimate the viscous dissipation associated with these micro-jets and to link it to acoustic absorption.

Keywords: *micro-perforated panel, acoustic absorption, streaming, time resolved PIV.*

**Corresponding author*: muriel.amielh@univ-amu.fr.

1. INTRODUCTION

Under the influence of the development of noise standards, research is being conducted to propose passive and lightweight solutions whose fouling can be resolved in the case of industrial applications such as in the design of aeronautical engine walls and compatible with efforts in the field of sustainable development. Micro-perforated panels consisting simply of holes or based on walls made of metamaterials ([1, 2]) are interesting solutions whose performance must be evaluated. Perforated walls have been particularly studied by Maa [3], for the sizing of holes for optimal efficiency. More recent work by Laurens et al. [4] has proposed an introductory synthesis which describes the three contributions of perforations to the acoustic behavior of a perforated panel. The assumptions made are that the porosity is less than 4% so that the interactions between the holes are neglected, which also amounts to having a large spacing between holes and that the acoustic wavelength is large compared to the characteristic dimensions of the perforations. Among the three physical phenomena mentioned, the first one is a non-viscous effect related to that the flow inside the hole behaves like a small air piston. It induces that, due to inertia effects, one has to consider in the acoustic models a length correction on the depth of the perforations. Then, it is necessary to take into account the viscous effects in the boundary layers which develop on the internal wall of the hole which will participate in the absorption of acoustic energy. Finally, in the presence of high amplitude sound waves striking the opening, a vortex detachment, which converts the acoustic energy

into mechanical energy, then dissipated into heat, can occur.

The present study aims to investigate experimentally the space-time behavior of the flow induced when MPP is subject to such high amplitude sound waves without mean flow. In the experiment, the sound is generated by a plane wave whose wave vector is parallel to the surface of the perforated panel, placed in the bottom of a close tube. Section 2 gives the set-up that allows the measurements of the flow velocity in the vicinity of apertures by high-speed PIV and the acoustic pressure measurements by microphone. Section 3 specifies the acoustic conditions chosen for the study. Results presented in Section 4 highlight and quantify the structure of the flow induced by pressure fluctuations.

2. EXPERIMENTAL SETUP

The MPP (Micro-Perforated Panel) is a perforated metal plate of $D = 100mm$ diameter and $1mm$ thickness. Three types of MPP (Fig. 1) are studied, whose periodic perforation characteristics are summarized in Tab. 1. Each MPP is successively installed above the same cavity located in the center of the floor of the Kundt tube. The diameter of the cavity is $100mm$ and its depth is $30mm$. The Kundt tube (Fig. 2) is a parallelepipedic volume of length $L_x = 1.06m$ and of square cross-section of side $L_x = L_z = 150mm$. Lateral walls are in glass and an optical access is possible on the top wall where the laser sheet is passing.

High-speed PIV (Particle Image Velocimetry) images are acquired and post-processed by a Dantec Dynamics system (RapiDO) that includes one T4040 SpeedSense Phantom high-speed camera ($2560\times1664\,pixels$, 12 bits), and a double pulsed laser. The camera is equipped with a $200mm$ focal lens with a $f\#4$ aperture in order to obtain good resolution on a small field of view in the vicinity of the MPP's surface. The pulsed laser is a Photonics laser (527nm, $2 \times 30mJ$ at a nominal $1kHz$ repetition rate). The DynamicStudio software controls the synchronization of image acquisition. A laser sheet generator constituted of several adapted lenses is installed at the end of the optical arm to illuminate the field of view of interest ($24.3mm \times 15.7mm$). 7000 PIV images are acquired at the frequency $F_s = 6.4kHz$ when the laser is working in a single mode, which means that the delay between two pulses is $1/F_s = 156\mu s$. The volume of the Kundt tube is seeded with olive oil droplets of $2-3\mu m$ diameter injected by a hole located on the upper wall. During seeding, the small hole located in the bottom wall of the cavity is left open so that droplets can flee when also pervading the cavity volume. In order to let the seeding stay in suspension, it is preventively stopped a few minutes before experiments with sound and the small hole located in the bottom wall of the cavity is closed. Thanks to the RapiDO system, the sound pressure inside the Kundt tube is measured synchronously with PIV using a wall microphone GRAS SC40. The microphone is located on the top wall at $\delta X = 55mm$ from the extremity wall. A loudspeaker is mounted on the opposite side.

Table 1. MPP dimensions.

MPP	d (mm)	i (mm)	Porosity
MPP1.0mm	1.12	5.15	2.5%
MPP0.6mm	0.65	4.30	1.4%
MPP0.3mm	0.30	1.87	1.5%

The spatial resolution for PIV is $\delta_x = \delta_y = 154\mu m$. The (O, X, Y, Z) coordinate system is centered on the middle of tube floor where the investigation is focused. The two instantaneous components ($2C$) of velocity (U, V) are measured on the plane ($2D$) $Z = 0$ specified in (Fig. 2) by a green square. Statistics and other post-processing of the 6999 velocity fields and acoustic signals are performed by homemade codes developed in Matlab.

3. CHARACTERIZATION OF THE KUNDT TUBE ENCLOSING THE MPP

3.1 Eigen modes of the Kundt tube

In order to investigate the flow induced by pressure fluctuations through the holes of the MMP, one chooses to generate a pressure field of high SPL (Sound Pressure Level) inside the Kundt tube. For that, the first eigen modes of the Kundt tube volume are first calculated and then checked by acoustic pressure measurement by the microphone for a white noise excitation in the range $200 - 3000Hz$ delivered by the loudspeaker. For this experiment, the microphone signal is acquired with a sample frequency of $25.6kHz$ during $100s$. The experimental frequencies of the modes are obtained by spectral analysis as shown in Fig. 3. The agreement between both series of eigen mode frequencies is quite good (Tab. 2). The retained frequencies for the following

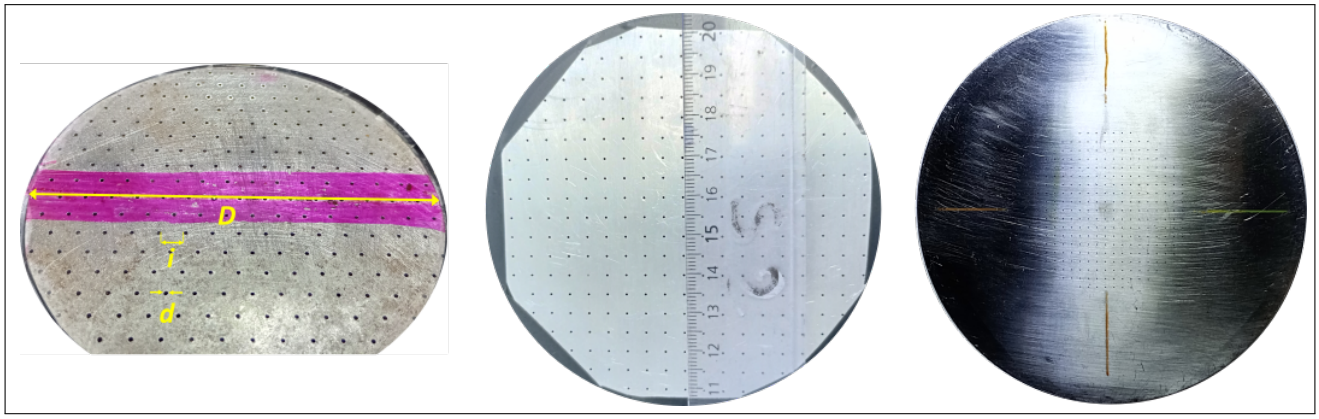

Figure 1. Disks of MPP, from left to right: MPP1.0mm, MPP0.6mm and MPP0.3mm.

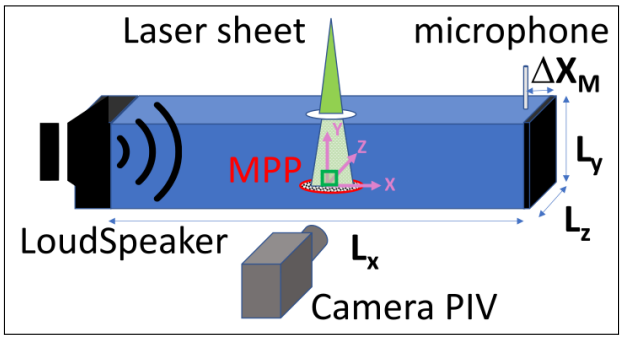

Figure 2. Setup of the high-speed PIV in the near field of MPP mentioned by the centered green square, the scheme is not scaled.

results correspond to the modes $(l, m, n) = (2, 0, 0)$ and $(3, 0, 0)$ along the respective direction (X, Y, Z). The associated frequencies will be named $F_2 = 324Hz$ and $F_3 = 486Hz$ hereafter. In this approach, the eigen modes of the cavity situated under the MPP, which are of higher frequencies, are not considered.

The two selected study frequencies allow to observe the behavior of the flow at the holes depending on whether the acoustic pressure is a node or an antinode. Fig. 4 gives a spatial representation of the amplitude of acoustic pressure in the Kundt tube. The scale of the geometry is respected and the PIV field of view is identified by a green rectangle above the red surface of the MPP centered on $(X = 0mm, Y = 0mm)$. For the long-wavelength $(2, 0, 0)$ and $(3, 0, 0)$ modes considered here, the microphone located at $\Delta X = 55mm$ from the closed end of the Kundt tube measures almost the maximum of the absolute value of the acoustic pressure amplitude.

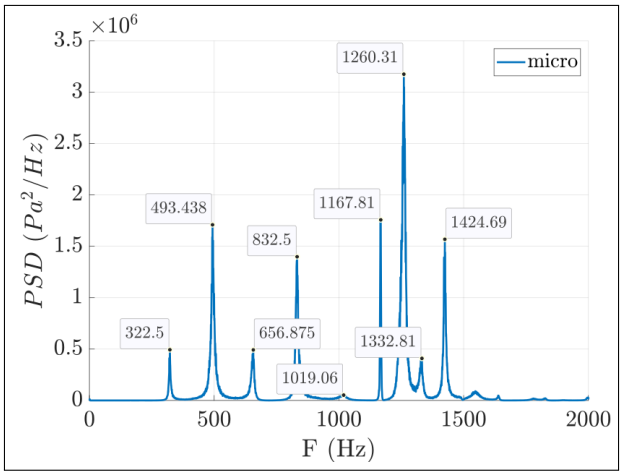

Figure 3. Spectral analysis of acoustic pressure measured by the microphone: experimental characterization of the first eigen modes of the Kundt tube by white noise excitation.

3.2 Measurement of the acoustic velocity by high-speed PIV

The case of the $(3, 0, 0)$ mode is investigated for a smooth wall for which the cavity is covered with a non-perforated

Table 2. Theoretical and experimental eigen modes of the Kundt tube.

l	m	n	$F_{l,m,n}$	F_{exp}
			(Hz)	(Hz)
1	0	0	162.1	-
2	0	0	324.2	322.50
3	0	0	486.29	493.44
4	0	0	648.39	656.88
5	0	0	810.49	832.50
6	0	0	972.59	1019.1
7	0	0	1134.7	1167.8
0	1 (0)	0 (1)	1143.3	-
1	1 (0)	0 (1)	1154.8	-
2	1 (0)	0 (1)	1188.4	-
3	1 (0)	0 (1)	1242.5	1260.3
8	0	0	1296.8	-
4	1 (0)	0 (1)	1314.4	1332.8
5	1 (0)	0 (1)	1401.5	-
9	0	0	1458.9	1424.7

metal plate. This configuration allows us to test whether we can measure the acoustic velocity with the PIV since for $F_3 = 486Hz$, the acoustic pressure is at a node above the MPP, but the amplitude of acoustic velocity is maximum. While measuring a standard deviation of $\sigma_P = 142.7Pa$ by microphone, a standard deviation σ_U of U velocity component, in the direction of plane wave vector generated by the loudspeaker, is measured by PIV. The spatial averaging of σ_U on the vertical direction Y at $X = 0mm$ gives $\sigma_U = 0.332m/s$ quite in a good agreement (4% error) with a theoretical estimation of the acoustic velocity by $\sigma_U = \sigma_P/(\rho c) = 0.347m/s$ with the sound speed $c = 343m/s$ and the air density $\rho = 1.2kg/m^3$. Similar measurements were made for $F_2 = 324Hz$ for which the theoretical acoustic velocity should be zero in the middle of the Kundt tube, one obtained a minimum of $\sigma_U = 0.013m/s$ on all the vertical line $X = -1.4mm$ in the PIV field of view.

Fig. 5 shows how the acoustic pressure signal measured at the Kundt tube end and the velocity components measured at X=0mm are timely synchronised. The signals of P, U and V are non-dimensionalized by their amplitude deduced from their standard deviation σ. All signals are harmonic. The V signal is of weak amplitude ($\sigma_V = 0.004m/s$) and very noisy comparatively to U signal for which $\sigma_U = 0.332m/s$. The phase shift between the velocity and the pressure is $\pi/2$ as it could be predict theoretically for a plane wave. These results indicate that PIV measurements give an applicable estimation of the acoustic velocity with the limitation of drag effects of seeding droplets.

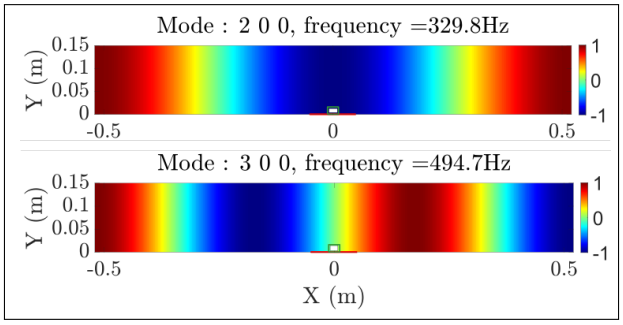

Figure 4. Theoretical acoustic pressure amplitudes for modes (l, m, n) = (2, 0, 0) and (3, 0, 0) of the Kundt tube.

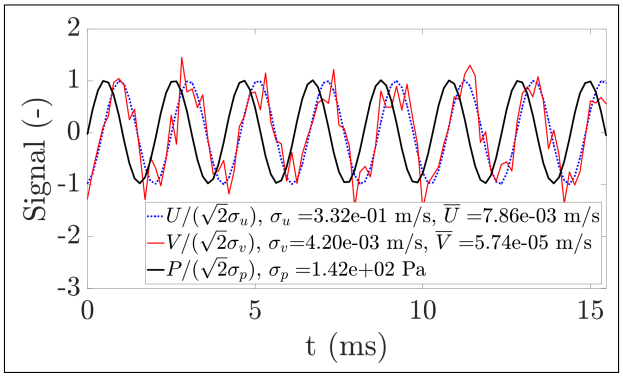

Figure 5. Time series of velocity components (U, V), extracted at position $(X = 0mm, Y = 5mm)$ in the PIV field of view for the smooth wall, and pressure signal measured synchronously by microphone, for $F_3 = 486Hz$ corresponding to a an acoustic pressure node at this place.

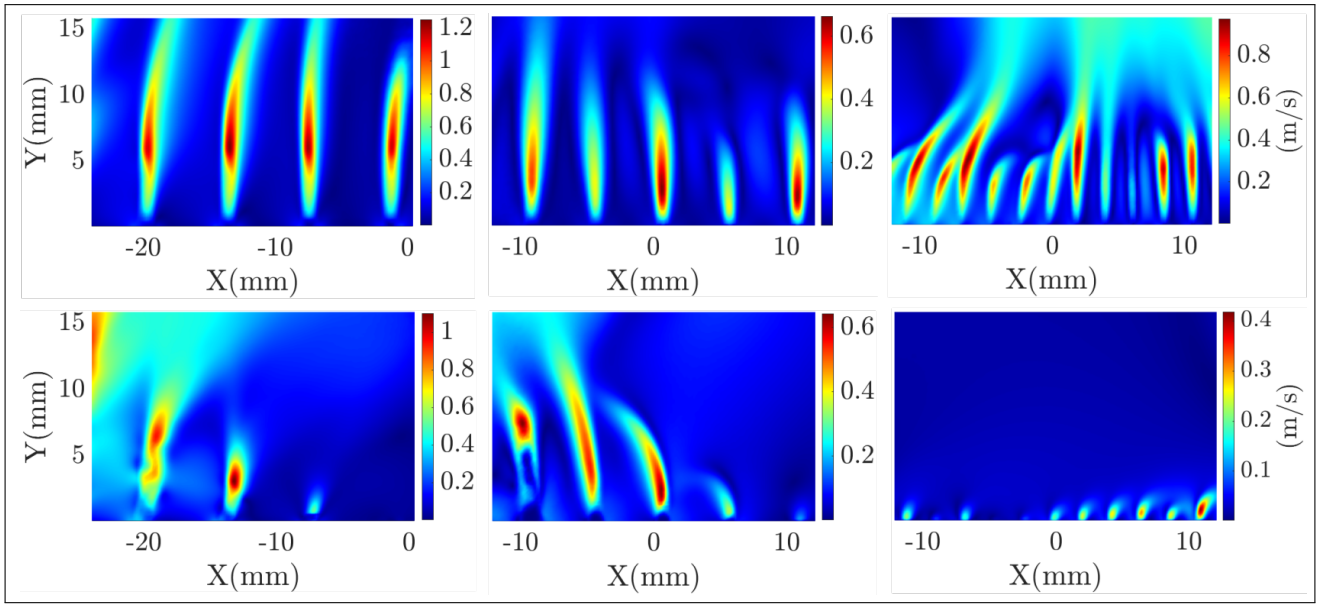

Figure 6. Mean velocity norm $\sqrt{\overline{U}^2 + \overline{V}^2}$ for MMP1.0mm, MPP0.6mm and MPP0.3mm from left to right. Top: for a antinode acoustic pressure (acoustic velocity node) over the MPPs, for $F_2 = 324Hz$. Bottom: for a acoustic pressure node (acoustic velocity antinode) over the MPPs , for $F_3 = 486Hz$.

4. EVIDENCE OF THE STREAMING

The mean velocity norm fields, obtained for all the MPPs, for both excitation frequencies $F_2 = 324Hz$ and $486Hz$, are presented in Fig. 6. The sound pressure levels associated to these PIV experiments are given in (Tab. 3). These results aim to compare the flow behaviour according to the existence of a node or antinode of acoustic pressure above the MPP. The influence of pressure is obvious. For conditions of pressure antinode ($F_2 = 324Hz$), the persistence of an average flow in the form of vertical jets escaping from the holes up to around $Y = 15d$ is an evidence of streaming. Contrariwise, for conditions of pressure antinode ($F_2 = 486Hz$), one observes an extinction of these jets in regions around $X = 0mm$. Remaining average jets have shorter vertical development than for $F_2 = 324Hz$ and seem to be submitted to transverse effects, possibly related to large scale streaming in the Kundt tube. At $F_2 = 324Hz$, the maxima of mean velocity norm occur at $Y/d = 5-6$ for MPP1.0mm and MPP0.6mm and rather at $Y/d = 15$ for MPP0.3mm. In this last case, the jets are not all active and those which have the greater vertical development interact in their far field. The standard deviation of V, not shown here, is maximum , respectively σ_v =0.46, 0.35, 0.49 m/s for the three MPPs, in the jet near field and becomes very weak in the region where the mean velocity norm becomes maximal. Beyond this region, the mean movement becomes predominant relatively to the fluctuating one.

Table 3. Sound Pressure Level (SPL) measured by the microphone with loudspeaker excitation.

SPL for	$F_2 = 324Hz$	$F_4 = 486Hz$
Smooth wall	133.7 dB	137.1 dB
MPP1.0mm	132.1 dB	140.2 dB
MPP0.6mm	129.2 dB	134.6 dB
MPP0.3mm	127.1 dB	133.9 dB

5. DYNAMICS OF THE FLOW

5.1 Spectral analysis

Fig. 7 presents a comparison of the spectral analyses of the acoustic pressure and the V velocity signal extracted

on the axis, in the near field, of one jet for the MPP1.0mm at $F_2 = 324Hz$. For the velocity signal, the excitation frequency and its harmonics are detected. However, the raw instantaneous PIV fields are noisy as shown by an extracted sample of V time series in Fig. 9, so a method is proposed herafter in order to fix the main contributions to the flow dynamics.

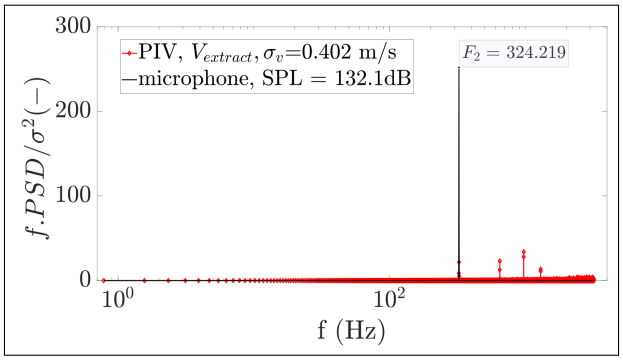

Figure 7. Spectral analysis of the pressure measured by microphone and V velocity components extracted from the PIV field at position $(X = 4.5mm, Y = 5mm)$ corresponding to an axial position on an ejected jet from a hole of MPP1.0mm at $F_2 = 324Hz$.

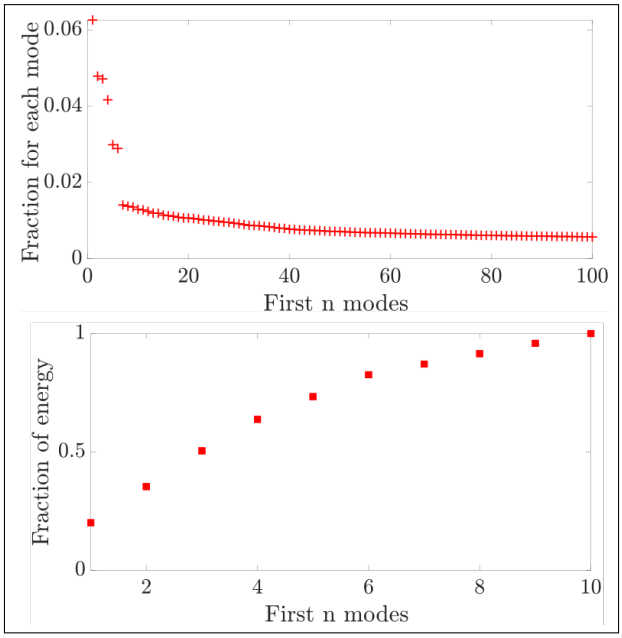

Figure 8. Fraction of energy associated to POD mode decomposition. Top: Ratio of energy for each considered mode to the cumulative energy of the first 100 modes. Bottom : Ratio of the cumulative energy for the n first modes to the cumulative for the first 10 modes.

5.2 POD of the velocity field

In order to highlight the space-time structure of the jets, one proposes to apply POD (Proper Orthogonal Decomposition, [5]) method which interest is to capitalize on the high amount of available fluctuating velocity fields. The principle of this method is to decompose the quantity of interest, here the velocity components, on a basis of eigen modes sorted by their energetic contribution. The decomposition is performed on 2000 uncorrelated snapshots of the two velocity components (U, V), which determines a number of modes equal to the number of realizations.

Fig. 8 illustrates how the energy is distributed according to the considered POD modes. The top figure shows the energetic contribution of each n mode to the cumulative energy of the first 100 modes. The first 6 modes are the main contributors comparatively to the all following ones. The ratio of the cumulative energy for n first modes to the cumulative for the first 10 modes presented in the bottom figure helps to specify that 64% or 83% cumulative energy is obtained by the contributions of the 4 or 6 first POD modes, respectively.

The space-time reconstruction of the instantaneous velocity field with the first 4 POD modes is proposed in Fig. 9 for a chosen jet ejected from one hole of the MPP1.0mm with the $F_2 = 324Hz$ excitation. The six snapshots presented in the top figure from the left to the right are associated to the instants $t_i = t_0, ..., t_5$ marked on the pressure time series plotted in the bottom figure for a duration covering at least one excitation period. According to the spatial representation of the theoretical mode (2,0,0) given in Fig. 4 the amplitude of the acoustic pressure over the MPP is of opposite sign to that can be measured by the microphone at Kundt tube end. So the non-dimensionalized signal of the velocity V extracted at the jet exit is plotted synchronously with the -P signal in order to analyse the flow dynamics in term of pressure fluctuations in the region of the MPP. When the acoustic pressure is negative, at t_1, a hemispherical flow burst is ejected from the hole. This burst continues to rise in the jet column and takes a spherical shape while, between t_2 and t_3,

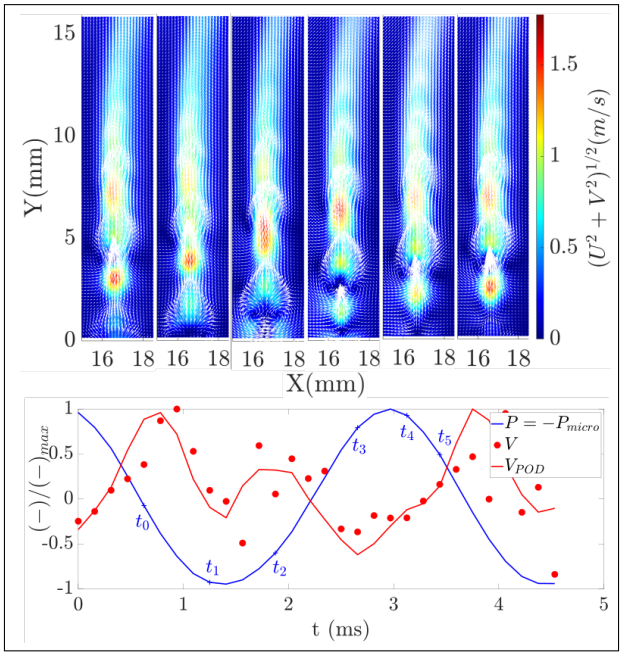

Figure 9. Top: Temporal evolution of the POD [1 2 3 4] velocity field for one jet ejected from a hole of the MPP1.0mm during a period for $F_2 = 324Hz$ excitation (acoustic pressure antinode over the MPP). The colorbar corresponds to the instantaneous velocity norm while the vectors are (U, V). Bottom : Times series of acoustic pressure measured by microphone synchronously with PIV. The vertical velocity component signal (V: raw PIV and V_{POD}: POD reconstruction) is extracted at the center of jet exit cross-section (position : $X = 16.6mm$, $Y = 0.15mm$)

pressure becomes zeros and flow stops moving at the hole exit. When the acoustic pressure is positive, the flow is reverse with negative V velocity in the hole near field and enters the hole as seen in velocity snapshots at t_3 and t_4. This behavior is repetitive over all pressure cycles.

The rotational aspect of the flow in the field of view suggests to calculate the vorticity using the POD reconstructed velocity vectors. Thanks to the high spatial resolution of (U, V) field, the out-plane instantaneous vorticity component:

$$\omega_z(X,Y,t) = \frac{\partial V(X,Y,t)}{\partial x} - \frac{\partial U(X,Y,t)}{\partial y} \qquad (1)$$

can be estimated. This is done with the first 6 POD mode reconstruction of (U, V) for the MPP1.0mm at $F_2 = 324Hz$.
Fig. 10 illustrates a snapshot of the fluctuating vorticity:

$$\omega'_z(X,Y,t) = \omega_z(X,Y,t) - \overline{\omega}_z(X,Y) \qquad (2)$$

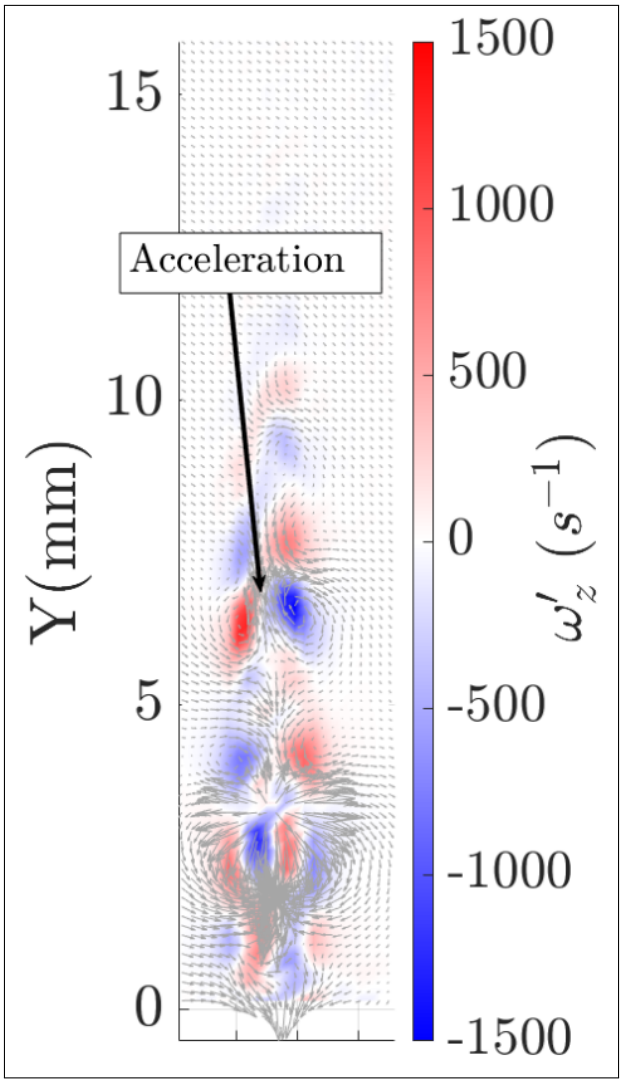

Figure 10. Snapshot of fluctuating vorticity component ω'_z and instantaneous velocity vectors (U,V) calculated from velocity field reconstructed with the six first POD modes for $F_2 = 324Hz$ excitation (acoustic pressure node over the MPP1.0mm).

This representation associated to the plotting of the

synchronous instantaneous velocity vectors underlines the symmetry of the flow on either side of the vertical axis of the jet. The snapshot is chosen for a positive acoustic pressure at the instant t_3 so that the flow entering the hole is clearly observable. Successive counter-rotating vortices are distributed along this symmetry axis. At $Y = 3.5mm$, it is clear that this $2D$ representation gives only a partial view of the $3D$ flow behavior. At $Y = 6mm$, two counter-rotating vortices with the largest magnitude of vorticity detected in the field of view induce an ascending vertical flow acceleration which could be the motor of the jet streaming since the maximum mean velocity is detected in this region as seen for the MPP1.0mm on the top figure of Fig. 6.

6. CONCLUSION AND PERSPECTIVES

The flow induced by high acoustic pressure levels at the apertures of MPP was investigated by measurements of velocity with high-speed PIV associated to synchronous measurements of acoustic pressure by microphone. When the MPP region is submitted to an acoustic pressure antinode, the flow is in the form of pulsated jets which could expand vertically above the aperture up to $Y/d = 15$. Thanks to a POD decomposition of the velocity field, the space-time structure of these jets is quantitatively characterized. The origin of a vertical streaming in the development region of the jet is guessed to be related to the presence of high vorticity counter-rotating vortices located at the end of the region above the apertures where the flow go out or in the perforation. The next step of the study is to quantify the loss of energy induced by this rotational aspect of the flow.

7. ACKNOWLEDGMENTS

The IRPHE technical staff is acknowledged for the design of the Kundt tube.
The high-speed stereo PIV system RapiDO is a funded project of A*Midex (Aix Marseille University).

8. REFERENCES

[1] C. Maury, T. Bravo, D. Mazzoni, M. Amielh, and L. Pietri, "Cost-efficient characterization of the aeroacoustic performance of micro-perforated wall-treatments in a wind tunne," in *Proc. of 179th Meeting of the Acoustical Society of America, POMA Volume 42*, (Virtually Everywhere), 2020.

[2] C. Maury and T. Bravo, "Vibrational effects on the acoustic performance of multi-layered micro-perforated metamaterials," *Vibration*, vol. 6, p. 695–712, 2023.

[3] D.-Y. Maa, "Potential of microperforated panel absorber," *Journal of the Acoustical Society of America*, vol. 104, no. 5, pp. 2861–2866, 2010.

[4] S. Laurens, E. Piot, A. Bendali, M. Fares, , and S. Tordeux, "Effective conditions for the reflection of an acoustic wave by low-porosity perforated plates," *Journal of Fluid Mechanics*, vol. 743, pp. 448–480, 2014.

[5] G. Berkooz, P. Holmes, and J. Lumley, "The proper orthogonal decomposition in the analysis of turbulent flows," *Annual Review of Fluid Mechanics*, vol. 25, p. 539–575, 1993.